Synthesis and characterization of 1D Co/$CoFe_2O_4$ composites with tunable morphologies†

Lijun Zhao, Hongjie Zhang,* Liang Zhou, Yan Xing, Shuyan Song and Yongqian Lei

Received (in Cambridge, UK) 26th March 2008, Accepted 24th April 2008
First published as an Advance Article on the web 9th June 2008
DOI: 10.1039/b805029e

1D Co/$CoFe_2O_4$ composites with tunable morphologies were fabricated by a facile solvothermal route in the presence of a surfactant poly(vinylpyrrolidone) (PVP); they may be very attractive for potential applications because of their outstanding soft magnetism.

The study of spinel ferrites is of great importance from both fundamental and applied research points of view. $CoFe_2O_4$ ferrite is of considerable interest because of its structural, magnetic and electrical properties.[1–4] One-dimensional (1D) magnetic materials are expected to have interesting properties, as the geometrical dimensions of the material become comparable to a key magnetic length scale, such as the exchange length or the domain wall width.[5] As a consequence, highly anisotropic 1D magnetic materials have been fabricated by a variety of methods, such as electrospinning (Co and Fe nanofibers),[6] thermal decomposition (CoO nanorods),[7] external magnetic field assisted solution-phase process (Ni chainlike nanowires),[8] template high-temperature reduction (ferrite nanowires and nanocables),[9,10] pulsed laser assisted vapor–liquid–solid deposition (ferrite nanorods, nanowires and nanobelts),[11] and iron–water reaction (iron oxide nanobelts).[12] However, what is lacking currently is a simple chemical route to fabricate low-dimensional magnetic materials with outstanding magnetic properties. Furthermore, for the synthesis of metal materials, it is necessary to use a reducing agent, or alternatively the whole reaction has to be kept under an inert atmosphere. In this communication, 1D Co/$CoFe_2O_4$ composites were fabricated by a facile solvothermal method without any inert gas protection and purification steps. The starting materials in this experiment are cheap and nontoxic and the experimental process is straightforward and environmentally friendly.

All chemicals were of analytical grade and were used as received without further purification. In a typical procedure, $FeSO_4{\cdot}6H_2O$ (0.154 g), of $CoCl_2{\cdot}6H_2O$ (0.066 g), of poly(vinylpyrrolidone) (PVP, MW 40 000) (0.5 g), were first added to the solution of distilled water (10 mL) and glycerol (30 mL) at room temperature, followed by the addition of NaOH (1.2 g) under stirring. The resulting solution was transferred into a 50 ml Teflon-lined autoclave, and maintained at 200 °C for 72 h, then air-cooled to room temperature. The solid products were collected by magnetic filtration and washed several times with water and ethanol. The final product was dried in a vacuum oven at 40 °C for 6 h.

Fig. 1(a) shows scanning electron microscopy (SEM) images of 1D Co/$CoFe_2O_4$ nanobelts. The belts are approximately 5 μm long and 50–300 nm wide. Their thicknesses are about 50 nm. The X-ray diffraction (XRD) pattern of the nanobelts (Fig. 1(b)) can be indexed to the face-centered cubic spinel phase of $CoFe_2O_4$ ferrite (JCPDS 22-1086). Peaks marked with an asterisk correspond to face-centered cubic Co metal (JCPDS 15-0806). Glycerol acts as both reducing agent as well as solvent; at high temperature and high pressure the α-H of glycerol can show strong reductive activity. The sharpness of the X-ray diffraction peaks indicates that the material is highly crystalline. Transmission electron microscopy (TEM, Fig. 1(c)) and high-resolution TEM (HRTEM, Fig. 1(d)) provide further insight into the microstructural details of the beltlike nanostructures. Fig. 1(d) shows a representative HRTEM image of the edge area of the Co/$CoFe_2O_4$ nanobelt. This image reveals that the nanobelt is composed of single-crystalline $CoFe_2O_4$ ferrite with interplanar spacing of about 0.29 nm, which corresponds to the (220) crystalline plane, and single-crystalline Co metal with interplanar spacing of about 0.17 nm, which corresponds to the (200) crystalline plane. Energy dispersive X-ray spectroscopy (EDX) (inset in Fig. 1(c)) recorded from superstructures revealed that the nanobelts are composed of Co, Fe and O. PVP plays a key

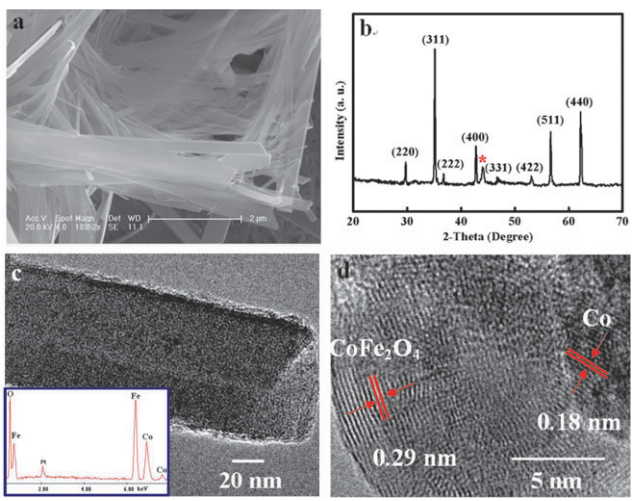

Fig. 1 (a) SEM image, (b) XRD pattern of Co/$CoFe_2O_4$ nanobelts, (c) TEM image and (d) HRTEM image of a single nanobelt. The inset in Fig. 2(c) is an EDX image of nanobelts.

State Key Laboratory of Rare Earth Resource Utilizations, Changchun Institute of Applied Chemistry, Chinese Academy of Sciences, Renmin Street No. 5625, Changchun, 130022, P. R. China. E-mail: hongjie@ciac.jl.cn; Fax: (+86)431-5698041; Tel: (+86)431-5262127

† Electronic supplementary information (ESI) available: XRD and EDX patterns of Co/$CoFe_2O_4$ composites prepared under different quantities of NaOH, and details of electrical measurements. See DOI: 10.1039/b805029e

role in the formation of the belt-like structure of the $Co/CoFe_2O_4$ composites. Use of 0.5 g of PVP is optimal for the fabrication: using lower amounts, octahedral particles and nanobelts were coexistent; while higher than this value, only octahedral nanoparticles were obtained. A further detailed report on the effect of the quantities of PVP used and solvothermal temperature on the morphologies of 1D $Co/CoFe_2O_4$ composites will be reported in a full paper.

To clarify the transformations of microstructural cobalt in different concentrations of NaOH, we further studied samples obtained with higher quantities of NaOH using SEM, XRD and EDX. SEM investigations show that the quantities of NaOH determine the morphologies of the $Co/CoFe_2O_4$ composites. From nanobelts to microcables, microcables with a few octahedra, and microcables with octahedra, the morphologies of $Co/CoFe_2O_4$ composites are changed by incrementally adjusting the quantities of NaOH (2–4 g) in glycerol (Fig. 2). For spinels that are characterized by an isotropic crystal structure (face-centered cubic lattice), symmetry breaking is required in the nucleation step to induce anisotropic growth. Meanwhile, the symmetry of a seed or the environment around a seed must be lowered to produce structures with 1D morphology. The presence of OH^- ions in the metal-ion–polyol system may act as a catalyst for accelerating the reduction reaction; they also act as a capping reagent, which kinetically controls the growth rates of various faces of the solid thus leading to anisotropic growth. In our case, we believe that the growth of the 1D $Co/CoFe_2O_4$ composites is based on an aggregation mechanism. That is, uniform $Co/CoFe_2O_4$ nanoparticles are formed under the solvothermal process; then the resulting $Co/CoFe_2O_4$ nanoparticles rotate and rearrange to minimize the surface energy. Finally after recrystallization 1D $Co/CoFe_2O_4$ composites result. The concentration of NaOH can modify the growth kinetics of the growing crystal, and a higher concentration of OH^- ions (*i.e.* higher chemical potential) in the solution may be responsible for the presence of octahedra.[13] We speculate that the PVP chain molecule, the chemical potential of solution, and magnetic dipole–dipole attraction all contribute to the assembly of octahedra onto the surface of the microcables. The diffraction peaks in XRD patterns (ESI†) for $Co/CoFe_2O_4$ composites synthesized with different NaOH quantities can be indexed to three phases: the diffraction peaks marked with black squares represent the face-centered cubic spinel phase of $CoFe_2O_4$ (JCPDS 22-1086); the peaks marked with blue spheres are hexagonal packed Co metal (JCPDS 05-0727)]; the peaks marked with red pentagrams are face-centered cubic Co metal (JCPDS 15-0806). With the increase in the concentration of NaOH, the intensities of diffraction peaks for $CoFe_2O_4$ ferrite are gradually decreased while the intensities of diffraction peaks for cobalt metal are gradually increased. EDX patterns of 1D $Co/CoFe_2O_4$ composites (ESI†) recorded from superstructures reveal that the composites are composed of Co, Fe and O. The contents of Co metal are increased with an increase of alkali concentration, as established by XRD and EDX patterns and the measurement results on a superconducting quantum interference device (SQUID) (below).

Fig. 3 shows the room-temperature hysteresis loop for the 1D $Co/CoFe_2O_4$ composites. The single-crystalline $Co/CoFe_2O_4$ nanobelts have high saturation magnetization (M_s = 109 emu g^{-1}) and moderate coercive force (H_c = 372 Oe). The high saturation magnetization of the nanobelts may be due to the presence of the Co metal in the $CoFe_2O_4$ ferrite. With the further increase of Co metal concentration in the ferrite, the saturation magnetization is increased while the coercive force is decreased. The saturation magnetizations for $Co/CoFe_2O_4$ composites with the morphologies of microcables, microcables with a few octahedra, and of microcables with octahedra are 150, 152 and 155 emu g^{-1} with corresponding values of coercivities of 1.7, 1.3 and 0.8 Oe, respectively. The high M_s and very low H_c indicate that the Co metal is predominant in the $Co/CoFe_2O_4$ composites. The soft magnetism of our obtained 1D magnetic composites are much superior than those reported elsewhere.[6,11,14]

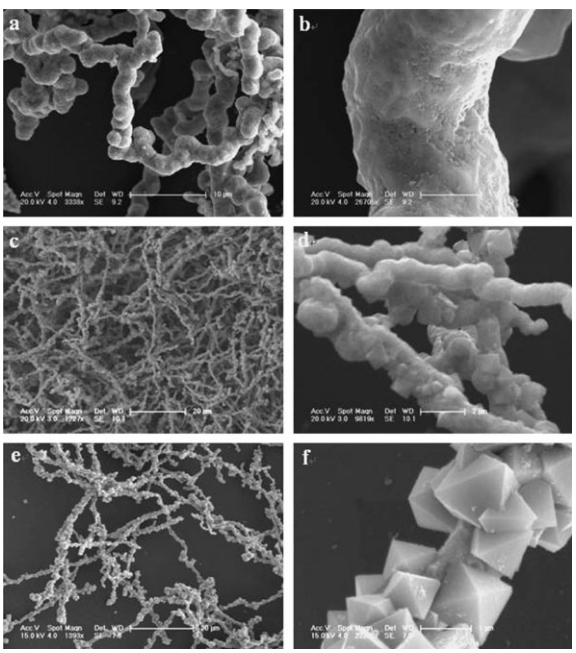

Fig. 2 Low-magnification SEM images of $Co/CoFe_2O_4$ composites synthesized with different quantities of NaOH: (a) 2 g, (b) 3 g, (c) 4 g. (d), (e) and (f) are the corresponding high-magnification SEM images.

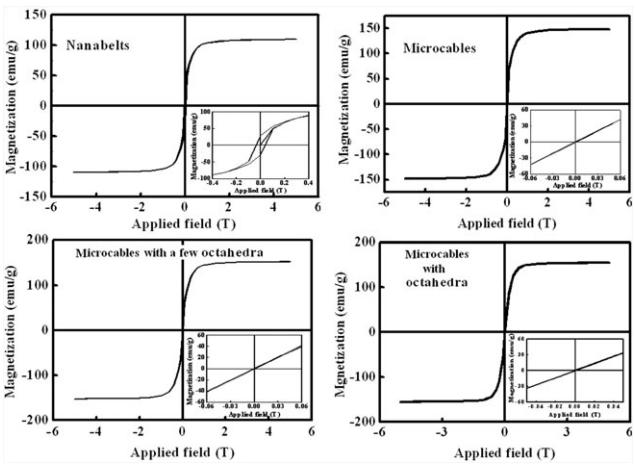

Fig. 3 Room-temperature hysteresis loop of 1D $Co/CoFe_2O_4$ composites. The inset is a magnified view of the hysteresis loop at low applied fields.

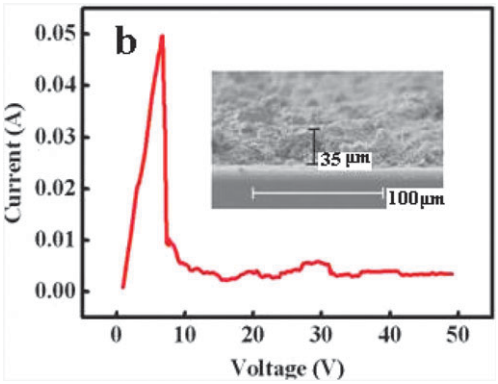

Fig. 4 *I–V* characteristics from a magnetic film consisting of Co/$CoFe_2O_4$ nanobelts. Inset: SEM image of the film in edge view showing the thickness of 35 μm.

We also carried out current–voltage (*I–V*) studies to investigate the electrical properties of the 1D Co/$CoFe_2O_4$ nanobelts (Fig. 4). Details of electrical measurement are shown in ESI.† Powders of Co/$CoFe_2O_4$ nanobelts dispersed in ethanol solution as building blocks were dropped directly on the substrate of the in-house device, and formed an electric film. The inset in Fig. 4 shows that the average thickness of the film is around 35 μm. The almost linear *I–V* curve from 0 to 6.8 V in Fig. 4 indicates a good ohmic contact behaviour between the film and Cu electrodes. A relatively high resistivity (43 Ω m) for the film of the single-crystalline Co/$CoFe_2O_4$ nanobelts may be owing to the presence of a contact potential between the metal and semiconductor. Further, the built-in electrical field counteracts part of the applied electrical field. The current decreases abruptly from 0.05 to 0.002 A at 6.8 V, which is probably because of the film is sensitive to the applied voltage. When the voltage or the current reaches a certain value, the film produces piezoresistance, but this differs from traditional piezoresistance. More detailed studies are currently being carried out to understand the mechanism. It is exciting that this abnormal electrical characteristic for the film of the single-crystalline Co/$CoFe_2O_4$ nanobelts is reproducible in our experiments.

In conclusion, we have developed a facile solvent–thermal route for the synthesis of 1D magnetic materials. PVP and OH^- ions act as shape controllers in the synthesis process. The Co metal content in the $CoFe_2O_4$ ferrite can be adjusted by the concentration of NaOH. The single-crystalline Co/$CoFe_2O_4$ nanobelts show outstanding magnetic properties and unique electrical properties while the 1D Co/$CoFe_2O_4$ composites exhibit outstanding soft magnetism.

The authors are grateful to the financial aid from the National Natural Science Foundation of China (Grant No.: 20631040) and the MOST of China (Grant No.: 2006CB601103). Lijun Zhao gratefully acknowledges Hong Kong (2007), the 40th China Postdoctoral Science Foundation and Training Fund of NENU'S Scientific Innovation Project.

Notes and references

1. A. Trestman Matts, S. E. Dorris, S. Kumarakrishnan and T. O. Mason, *J. Am. Ceram. Soc.*, 1983, **66**, 829.
2. A. H. Latham, R. S. Freitas, P. Schiffer and M. E. Williams, *Anal. Chem.*, 2005, **77**, 5055.
3. A. D. D. Broemme, *IEEE Trans. Electron. Insul.*, 1991, **26**, 49.
4. H. Mohan, I. A. Saikh and R. G. Kulkarni, *Solid State Commun.*, 1992, **82**, 907.
5. (*a*) M. Hehn, E. Jouguelet, K. Ounadjela, I. Petej, I. L. Prejbeanu and M. J. Thornton, *J. Phys.: Condens. Matter*, 2002, **14**, R1175; (*b*) Y. Henry, K. Ounadjela, L. Piraux, S. Dubois, J. M. George and J. L. Duvail, *Eur. Phys. J. B*, 2001, **20**, 35.
6. M. Graeser, M. Bognitzki, W. r. Massa, C. Pietzonka, A. Greiner and J. H. Wendorff, *Adv. Mater.*, 2007, **19**, 4244.
7. K. An, N. Lee, J. Park, S. C. Kim, Y. Hwang, J.-G. Park, J.-K. Kim, J.-H. Park, M. J. Han, J. Yu and T. Hyeon, *J. Am. Chem. Soc.*, 2006, **128**, 9753.
8. (*a*) G. Q. Zhang, T. Zhang, X. L. Lu, W. Wang, J. F. Qu and X. G. Li, *J. Phys. Chem. C*, 2007, **111**, 12663; (*b*) L. X. Sun, Q. W. Chen, Y. Tang and Y. Xiong, *Chem. Commun.*, 2007, 2844.
9. M. T. Chang, L. J. Chou, C. H. Hsieh, Y. L. Chueh, Z. L. Wang, Y. Murakami and D. Shindo, *Adv. Mater.*, 2007, **19**, 2290.
10. B. Daly, D. C. Arnold, J. S. Kulkarni, O. Kazakova, M. T. Shaw, S. Nikitenko, D. Erts, M. A. Morris and J. D. Holmes, *Small*, 2006, **2**, 1299.
11. J. R. Morber, Y. Ding, M. S. Haluska, Y. Li, J. P. Liu, Z. L. Wang and R. L. Snyder, *J. Phys. Chem. B*, 2006, **110**, 21672.
12. Y. M. Zhao, Y. H. Li, R. Z. Ma, M. J. Roe, D. G. McCartney and Y. Q. Zhu, *Small*, 2006, **2**, 422.
13. X. M. Liu, S. Y. Fu and H. M. X, *Mater. Lett.*, 2006, **60**, 2979.
14. L. Guo, F. Liang, X. G. Wen, S. H. Yang, W. Z. Zheng, C. P. Chen and Q. P. Zhong, *Adv. Funct. Mater.*, 2006, **17**, 425.

